J Fluoresc (2015) 25:1279–1296
DOI 10.1007/s10895-015-1616-z

ORIGINAL ARTICLE

A Study on Spectro-Analytical Aspects, DNA – Interaction, Photo-Cleavage, Radical Scavenging, Cytotoxic Activities, Antibacterial and Docking Properties of 3 – (1 – (6 – methoxybenzo [d] thiazol – 2 – ylimino) ethyl) – 6 – methyl – 3H – pyran - 2, 4 – dione and its Metal Complexes

Mudavath Ravi[1] · Kishan Prasad Chennam[1] · B. Ushaiah[1] · Ravi Kumar Eslavath[2] · Shyam Perugu[2] · Rajanna Ajumeera[3] · Ch. Sarala Devi[1]

Received: 26 March 2015 / Accepted: 5 July 2015 / Published online: 28 August 2015

Abstract The focus of the present work is on the design, synthesis, characterization, DNA-interaction, photo-cleavage, radical scavenging, in-vitro cytotoxicity, antimicrobial, docking and kinetic studies of Cu (II), Cd (II), Ce (IV) and Zr (IV) metal complexes of an imine derivative, 3 – (1 – (6 – methoxybenzo [d] thiazol – 2 – ylimino) ethyl) – 6 – methyl – 3H – pyran – 2, 4 – dione. The investigation of metal ligand interactions for the determination of composition of metal complexes, corresponding kinetic studies and antioxidant activity in solution was carried out by spectrophotometric methods. The synthesized metal complexes were characterized by EDX analysis, Mass, IR, ^{1}H-NMR, ^{13}C-NMR and UV–Visible spectra. DNA binding studies of metal complexes with Calf thymus (CT) DNA were carried out at room temperature by employing UV-Vis electron absorption, fluorescence emission and viscosity measurement techniques. The results revealed that these complexes interact with DNA through intercalation. The results of in vitro antibacterial studies showed the enhanced activity of chelating agent in metal chelated form and thus inferring scope for further development of new therapeutic drugs. Cell viability experiments indicated that all complexes showed significant dose dependent cytotoxicity in selected cell lines. The molecular modeling and docking studies were carried out with energy minimized structures of metal complexes to identify the receptor to metal interactions.

Keywords DNA binding · Photo cleavage · Cytotoxicity · Antioxidant

Introduction

In the rapid developing area of metal-based chemotherapy, the designing of new drugs is potential field of research. The pioneer success of cisplatin for the treatment of cancer is an impetus to explore the activity of various other complexes in chemotherapy. It has been reported that cisplatin utility as an anticancer drug is limited to a narrow range of tumors because of side effects associated with these drugs [1–3]. The drug cisplatin is highly effective against testicular and ovarian carcinomas as well as bladder, head and neck tumors [4, 5]. Lippard and his co-workers had studied the detailed molecular mechanism of the interaction of cisplatin with a natural target DNA [4, 6, 7]. To overcome the side effects and limited clinical utility associated with this drug, the design of more efficient, less toxic and predominant anticancer drugs to target DNA is an important research in the area of chemotherapy in recent years [8–10]. The literature reveals that the imine base metal complexes have a wide range of applications as anticancer [11, 12], antibacterial and antifungal agents [13, 14]. The interaction of probable compounds with DNA occurs through three modes of binding viz; intercalation, groove

Electronic supplementary material The online version of this article (doi:10.1007/s10895-015-1616-z) contains supplementary material, which is available to authorized users.

✉ Ch. Sarala Devi
dr_saraladevich@yahoo.com

[1] Department of Chemistry, Osmania University, Hyderabad 500 007, Telangana, India

[2] Department of Bio-Chemistry, Osmania University, Hyderabad 500 007, Telangana, India

[3] National Institute of Nutrition, Hyderabad 500 007, Telangana, India

binding and external static electronic effect [15–18]. Among these, intercalation is of utmost importance and is confined to the antitumor activity of the compound. General anticancer agents of clinical use cause damage to the DNA, affecting DNA replication or inhibiting the hormonal stimulation of cancer cells, leading to the death of these cells [19–24]. Considerable research has been undergone in the development of anticancer drugs based on transition metal complexes which interact with DNA, due to their kinetic stability. Moreover their photochemical properties make them as potential probes of DNA structure and conformations [18, 21, 22]. In the recent years the selective permeability of the cancer cell membranes to copper complexes and their compact regulations of the intracellular concentration has encouraged the synthesis of copper-based drugs as potential anticancer agents that are projected to have less severe side effects [25]. Metal complexes of schiff base of planar benzothiazole ring having azomethine linkage [26] were found to exhibit various antibacterial, antifungal, herbicidal and clinical activities [27–29]. Electrophoretic mobility shift processes are widely used to examine the potency of DNA cleavage, as well as the thermodynamic and kinetic aspects of the reaction [30, 31]. In general the Cu (II) and Cd (II) complexes [32] that possess high nucleobase affinity are potential reagents for the cleavage of DNA both oxidatively [33, 34] and hydrolytically [31]. In the present investigation, we report the synthesis and characterization of novel ligand 3 – (1 – (6 – methoxybenzo [d] thiazol – 2 – ylimino) ethyl) – 6 – methyl – 3H – pyran – 2, 4 – dione, and its metal complexes with Ce (IV), Zr (IV), Cu (II) and Cd (II). Efforts were also made to study the photo cleavage, cytotoxicity, DNA binding, antimicrobial, scavenging activity aspects of above candidate compound and its complexes.

3-MBTMPD 3 – (1 – (6 –methoxybenzo [d] thiazol – 2 – ylimino) ethyl) – 6 – methyl – 3H pyran – 2, 4 – Dione, CT-DNA Calf thymus DNA, DMSO Dimethyl sulfoxide, ESI–MS Electrospray ionization mass spectrometry, IC_{50} Half-maximal inhibitory concentration, MLCT Metal-to-ligand charge transfer, LMCT Ligand-to-Metal- charge transfer, MTT 3-(4,5-Dimethylthiazol-2-yl)-2,5-diphenyltetrazolium bromide, DAPI 4′,6-Diamidino-2-phenylindole dihydrochloride, DPPH 2,2-Diphenyl-1-picrylhydrazyl, HeLa Human cervical cancer cell line, HEK293T Human Embryonic Kidney cell line, DHAA Dihydroacetic acid, EB Ethidium bromide, Tris Tris(hydroxymethyl)aminomethane, PBS Phosphate-buffered saline.

Experimental

Materials

All the chemicals and reagents used were of AR grade. Dehydroacetic acid (DHAA) and 2 – amino – 6 – methoxy benzothiazole, MTT dye and Calf thymus (CT) DNA, were procured from Sigma Aldrich Chemicals. HeLa human cervical carcinoma cell and human embryonic kidney 293 cells lines were obtained from NCCS, Pune and maintained in RPMI 1640 medium supplemented with 10% (*V/V*) fetal bovine serum, 2 mM L-glutamine, 4.5 g L^{-1} glucose. Super coiled pBR 322 plasmid DNA (stored at 253 K) was obtained from Fermentas Life Science. Experiments were conducted using double distilled and ultra pure Milli – Q water.

Synthesis and Characterization

Synthesis of 3-(1-(6-methoxybenzo [d] thiazol-2-ylimino) ethyl) -6-methyl-3H- pyran-2-4 dione 2-amino-6-methoxybenzothiazole (1.802 g, 10 mmole) and dehydroacetic acid (10 mmole) in ethanol (40 mL) were refluxed for 7–8 h at 333–353 K. The reaction mixture was monitored by TLC. After completion of the reaction, the yellow coloured solid product formed was filtered off and washed with ethanol, dried and purified by recrystallization from hot ethanol. Yield: 69 %. Mp: 503–523 K. Anal. Calcd for $C_{16}H_{14}N_2O_4S$: C, 53.83; H, 4.81; N, 8.43. Found: C, 54.32; H, 4.19; N, 8.41 %. ^{1}H NMR ($CDCl_3$ 400 MHz): δ/ppm 15.7 (s, 1H, OH), 2.16 (s, 3H, -N=C-CH_3), 7.12, 8.9 (d, s 3H, ArH), 6.12 (s, 1H, =C-H), 3.88 (s, 3H, -OCH_3), 2.54 (s, 3H, O-C-CH_3), 7.25 (s, $CDCl_3$). ^{13}C NMR ($CDCl_3$ 400 MHz): *δ* /(ppm) 125, 162, (6C, ArC), 120 (1C, -N=C), 125 (1C, thiozole C), 55.9 (1C, -O-CH_3), 24.92, 22.45 (2C -CH_3), 103, 106 (2 C, alkene C), 184, 191 (2C, ketone) and 30.089 (1C, N=C-C, DHAA ring attached carbon. IR (KBr, / cm^{-1}): $_{(OH)}$: 3363, $_{(C=N):}$ 1633, $_{(C-O):}$ 1220. UV-Vis (nm): 223, 273, 352, ESI-MS (m/z): Calcd: 330. Found: 331 [M+H].

Synthesis of [Cd (II) (L) (NO_3) (H_2O)]

A mixture of imine base L (3-MBTMPD) and Cd (II) nitrate in ethanolic solution (40 mL) was refluxed for 7–8 h at 333–353 K under N_2 atmosphere. The resulting solution was allowed to stand, the brown colored solid product obtained was filtered and recrystallised from hot ethanolic solution. The brown colored solid complex [Cd (II) -3-MBTMPD] obtained was dried in desiccator over anhydrous $CaCl_2$ Yield: 55 %. Mp: >573 K Anal. Cald for $C_{16}H_{15}CdN_3O_8S$: C, 36.64; H, 3.24; N, 8.01. Found: C, 36.55; H, 3.30; N, 8.12 %.^{1}H NMR (DMSO 400 MHz): δ/ppm 2.35 (s, 3H, -N=C-CH_3), 7.17 (s, 2H, Ar), 7.7 (s, 1H, Ar), 8.77 (s, 1H, Ar), 3.85 (s, 3H, -OCH_3), 2.54 (s, 3H, =C-CH_3). IR (KBr /cm^{-1}): $_{(H2O)}$: 3552, $_{(C=N)}$: 1627, $_{(C–O)}$: 1112, $_{(M–O)}$: 619, $_{(M–N)}$: 397. UV-Vis (*λ* nm): 230, and 297. ESI-MS (m/z): Calcd: 522. Found: 524 [M+2].

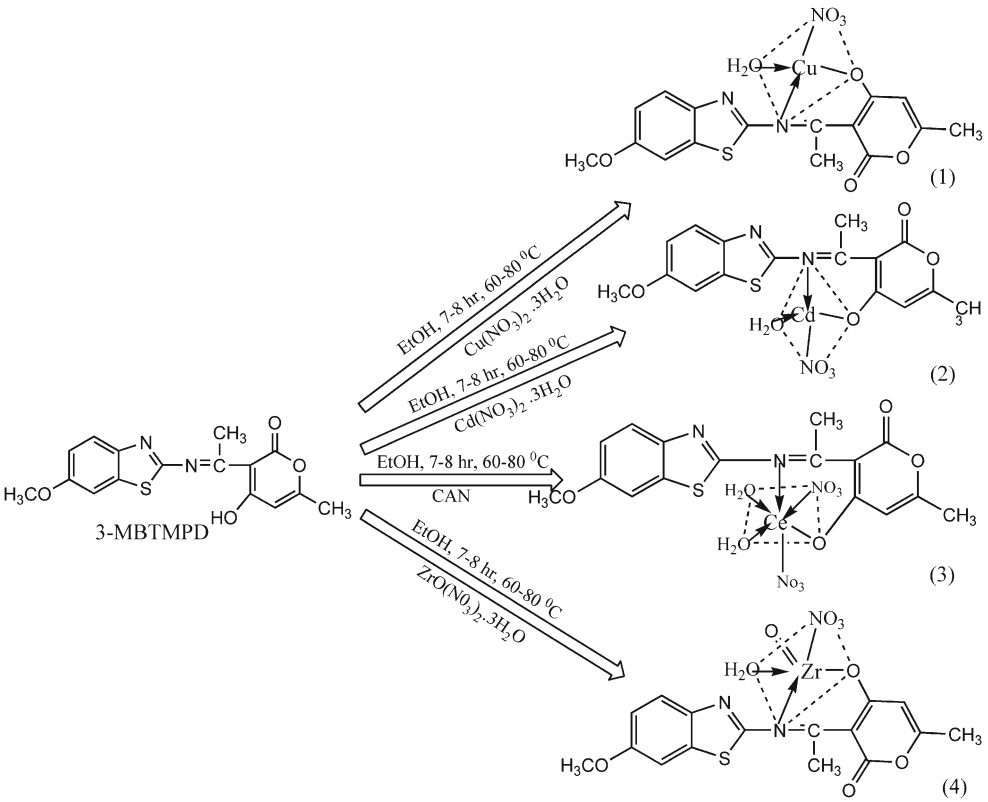

Fig. 1 Chemical structures of 3-MBTMPD and its metal complexes (1–4)

Synthesis of [Cu(II) (L) (NO_3) (H_2O)]

The imine base 3-MBTMPD (0.330 g, 1 mmole) and copper nitrate (1 mmole) were dissolved in ethanolic solution (40 mL) and then refluxed for 7–8 h at 333–353 K. The Light blue color product was obtained. The precipitate was filtered and washed with ethanol several times and dried in desiccator. Yield: 59 %. Mp: >573 K. Anal. Cald for $C_{16}H_{15}CuN_3O_8S$: C, 40.50; H, 3.61; N, 8.66. Found: C, 40.36; H, 3.79; N, 8.95 %. IR (KBr /cm^{-1}): $_{(H2O)}$: 3448, $_{(C=N)}$: 1573, $_{(C–O)}$: 1151, $_{(M–O)}$: 680, $_{(M–N)}$: 451. UV-Vis (nm): 226, 246, 410 and 567. ESI-MS (m/z): Calcd: 472. Found: 475 [M+3].

Synthesis of [Zr (IV) O (L) (NO_3) (H_2O)]

The metal complex was synthesized by mixing [$ZrO(NO_3)_2$. $2H_2O$)] (0.581 g, 1 mmole) with the equimolar ratio of the imine base (1 mmole) in 30 mL of ethanol. The mixture was refluxed for 7–8 h. The precipitated compound was collected by filtration and purified by washing with ethanol and dried under vacuum. Yield: 62 (%). Mp: >573 K Anal. Cald for $C_{17}H_{17}N_3O_9ZrS$: C, 33.10; H, 2.93; N, 9.65. Found: C, 34.08; H, 3.92; N, 9.93 %. IR (KBr /cm^{-1}): $_{(H2O)}$: 3411, $_{(C=N)}$:1602, $_{(C–O)}$: 1136, $_{(M–O)}$: 648, $_{(M–N)}$: 453. UV-Vis (nm): 235, 260, 342. ESI-MS (m/z): Calcd: 530. Found: 553 [M+Na].

Synthesis of [Ce (IV) (L) (NO_3) $_2$ (H_2O)$_2$]$^+$

The Ce (IV) complex was prepared by the addition of 1 mmole of the hot ethanolic solution of 3- MBTMPD (0.33 g in 50 mL ethanol) to 1 mmole of $[(NH_4)_2Ce(NO_3)_6]^{-2}$ and the solution was made 85 % *v/v* of ethanol /water. The pH of the mixture was adjusted in the range of 5.0–6.0 using alcoholic NH_4OH and then refluxed for 7–8 h with continuous stirring. The solid complex separated was filtered and washed with ethanol [35]. Yield: 61(%). Mp: >573 K. Anal. Cal for $C_{16}H_{17}CeN_4O_{12}S$: C, 35.37; H, 3.00; N, 8.86. Found: C, 38.35; H, 3.90; N, 9.56 %.^{1}H NMR (DMSO 400 MHz): δ/(ppm) 2.52 (s, 3H, -N=C-CH_3), 7.09-7.40 (s, 4H, Ar), 3.74 (s, 3H, -OCH_3), 2.07 (s, 3H, =C-CH_3). IR (KBr /cm^{-1}): $_{(H2O)}$: 3358, $_{(C=N)}$: 1618, $_{(C–O)}$: 1053, $_{(M–O)}$: 540, $_{(M–N)}$ 462. UV-Vis (nm): 214, 280, 347, 469. ESI-MS (m/z): Cald: 629. Found: 654 (M+Na+2H).

Physical Measurements

General Techniques

FT-IR spectra of the title compound and the corresponding metal complexes were recorded on Perkin Elmer – 337 Spectrophotometer with KBr pellets. Other instruments employed for characterization include – Perkin Elmer – 2400 Elemental Analyzer, Schimadzu UV-2600 spectrophotometer, Bruker –

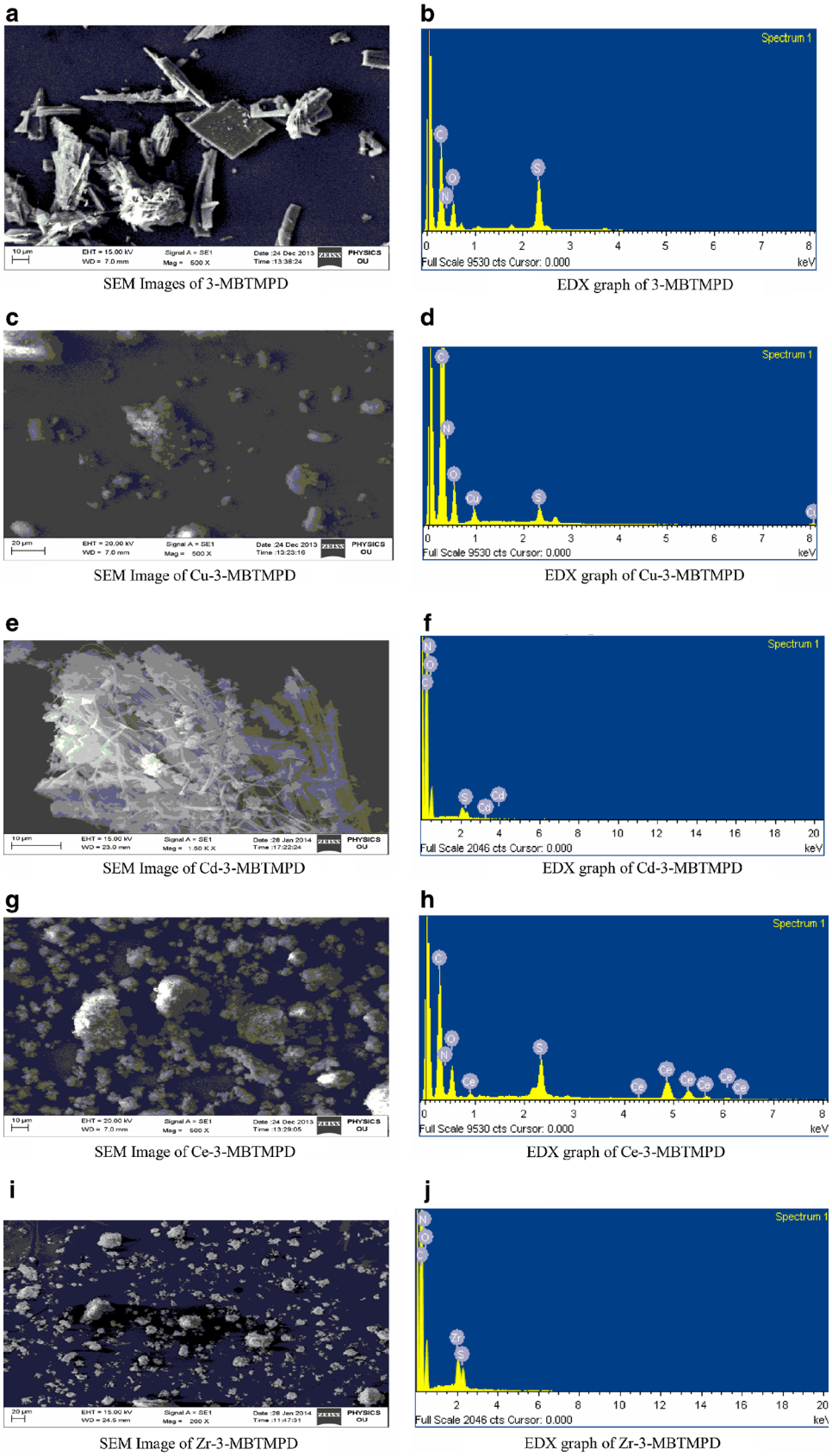

Fig. 2 SEM images and EDX graphs of [3-MBTMPD] (**a**–**b**), [Cu (II)-3-MBTMPD] (**c**–**d**), Cd(II) 3-MBTMPD] (**e**–**f**), [Ce (IV)-3-MBTMPD] (**g**–**h**) and [Zr (IV)-3-MBTMPD](**i**–**j**) complexes

Table 1 Second order rate constants for the formation of Cu (II) complex at different temperatures

Cu (II) complex Temp (K)	Equation	R^2	Rate constant (Lit $mole^{-1}$ min^{-1})	Actual rate constant (k_{obt} X ε)
Temp (K)				
288	y=0.0284x+4.8683	0.9844	0.0284	0.026838
298	y=0.0338x+4.6969	0.9981	0.0338	0.031941
303	y=0.0398x+4.5241	0.9667	0.0398	0.037611
308	y=0.0461x+5.1928	0.9872	0.0461	0.043565

Actual rate constant (k) = rate constant (obtained from graph) $_{\times}$ molar extinction coefficient (ε)

Avance-III 400 MHz ^{1}H and ^{13}C Fourier transform digital NMR spectrometer. RF-5301PC Spectrofluorophotometer, Confocal Microscope (LSM 510 META) Zeiss. Mass spectra were recorded on a VG – AUTOSPEC spectrometer. Melting point measurements were done on Polmon – MP – 96 instruments. Particle-size and morphology studies were carried out employing zeiss scanning electron microscope. Elemental analysis was done on the INCA EDX instrument. GeNei electrophoresis instrument was used for DNA cleavage studies.

Spectrophotometric Studies

Spectrophotometric technique is employed in the following experiments, viz; (i) for the determination of the composition of metal complex by Job's continuous variation and Mole ratio methods, (ii) for the determination of order of reaction in the formation of metal complex and thermodynamic parameters such as activation energy (E_a), entropy change (ΔS^*), free energy change (ΔG^*) and enthalpy change (ΔH^*) [36], (iii) for determination of antioxidant properties using 2, 2-diphenyl-picrylhydrazyl (DPPH) by in-vitro assay method [37], (iv) Binding ability of metal complexes with CT- DNA.

Determination of the Composition of Metal Complex

Spectrophotometric method is useful in studying equilibrium reactions for the formation of complexes in solution. The composition of metal complex can be ascertained by adjusting the appropriate pH of metal – ligand solution by suitable buffer solution to progress the complex formation. An attempt was made in present investigation to establish the metal to ligand ratio in Cu (II)- 3 – MBTMPD system. Metal to ligand ratio of the green colored complexes formed by the reaction between 3-MBTMPD and Cu (II) was studied by adopting Job's continuous variation and mole ratio methods.

Table 2 First order rate constant for the formation of copper (II) complex at room temperature

M (II) complex	Equation	R^2	Rate constant (min^{-1})
Cu (II)	y=−0.0006x+0.5972	0.9768	0.0006

Determination of Order Of Reaction of Cu (II) Complex

The experiment is carried out under (a) Pseudo first order reaction condition (1 mL 10^{-3} M (ligand)+1 mL 10^{-2} M Cu (II) +1 mL ethanolic ammonia buffer+7 mL dioxane) at 298 K and (b) second order reaction condition (1 mL 10^{-3} M (ligand)+1 mL 10^{-3} M Cu (II) +1 mL ethanolic ammonia buffer+7 ml dioxane at four different temperatures (288 K, 298 K, 303 K and 308 K).

Radical Scavenging Activity

The percentage of free radical scavenging activity is shown in Fig. 10. This assay is completely based on decrease in absorbance value of DPPH at 517 nm on addition of complex. The experiment involves diluting the working solution of the metal complexes and the ascorbic acid standard (700, 600, 500, 400, 300 and 200 μg μL^{-1}) in methanol. DPPH concentration was kept constant (2 mL, 0.004 %). To this varying concentration of metal complexes and standard were added. The mixture was shaken vigorously and kept in dark for 30 min at room temperature. Then the absorbance was measured at 517 nm in a spectrophotometer. The whole experiment was carried out using spectroscopic grade methanol solvent at 298 K. The radical scavenging activity has been measured by using the following Eq. 1;

$$\text{Suppression ratio } (\%) = [(A_0 - A_i)/A_0] \times 100\ \% \qquad (1)$$

Where A_i=the absorbance in the presence of the ligand or its complexes, A_0=the absorbance in the absence of the ligand or its complexes.

DNA Binding

DNA is the main genetic carrier and it is target to many metal based drugs. So, DNA binding study is one of the important steps for knowing the chemical nuclease activity of the metal complexes and enables to design effective DNA targeted metal based drugs. Electron absorption spectroscopy is one of the most important techniques for investigating the DNA binding studies at room temperature. The above synthesized

Table 3 Activation energy for the formation of copper (II) complex

M (II) complex	Equation	R^2	Activation energy (kJ $mole^{-1}$)
Cu (II)	y=−2.131x+7.815	0.970	17.72

complexes were demonstrated for DNA binding ability to explore their potential as DNA intercalators. The binding affinity of the metal complexes with CT-DNA was studied in tris (hydroxymethyl) aminomethane buffer (5 mM Tris-HCl, 50 mmole NaCl, pH: 7.2). A solution of CT-DNA in Tris-HCl buffer gives a ratio of UV absorbance at 250 nm and 260 nm of 1.8 : 1.0 to 1.9 : 1.0, indicating that the DNA was sufficiently free of protein [38]. The concentration of DNA per nucleotide was determined spectrophotometrically using molar absorptivity at 260 nm. Stock solutions of CT-DNA were stored at 269 K and used within 5 days. Concentrated stock solutions of metal complexes were prepared by dissolving calculated amount of metal complexes in DMSO and diluted with the corresponding buffer to the concentration required for all the experiments. The electron absorption titration of the complexes in buffer (Tris-HCl buffer) was carried out using a fixed metal complex (1–4) concentration, to which increasing order of the DNA stock solution was added. The solutions were incubated for 5 min before the absorption spectra were recorded. The binding strength of the complexes with DNA is calculated in terms of intrinsic binding constants K_b in respective systems by using the following Eq. 2 [39].

$$[DNA]/(\varepsilon_a-\varepsilon_f) = [DNA]/(\varepsilon_b - \varepsilon_f) + 1/K_b(\varepsilon_b - \varepsilon_f) \quad (2)$$

The apparent absorption coefficient ε_a, correspond to A_{obs}/[metal complex]. While the terms ε_f and ε_b corresponds to the extinction coefficient of the free metal complex (unbound) and the fully bound metal complex to DNA, respectively. K_b is given by the ratio of the slope to the intercept in a plot of [DNA] / (ε_a - ε_f) vs [DNA] for the titration of metal complex with DNA. In graph arrow shows the change in the absorption with increasing DNA concentration.

Fluorescence Quenching

To further support the binding strength of a metal complex (1–4) to CT-DNA, a competitive fluorescence quenching experiment was carried out using ethidium bromide (EB) bound CT-DNA solution in Tris-HCl buffer solution (pH: 7.10). Ethidium bromide (EB) is a common fluorescent probe [40] for DNA structure and has been used to examine the mode of DNA binding to a specific metal complex. Ethidium bromide (EB) shows the weak, reduced fluorescent intensity in Tris-HCl buffer solution (pH 7.10). But its fluorescence intensity is enhanced when bound to DNA due to intercalation into the base pairs of DNA. A competitive binding of the metal complexes to CT-DNA results in the displacement of the bound EB, thereby decreasing its emission intensity. The quenching constant (Kq) was calculated using the classical Stern-Volmer Eq. 3 [41].

$$I_0/I = K_q[Q] + 1 \quad (3)$$

Where I_0 is the emission intensity in the absence of quencher, I is the emission intensity in the presence of quencher, Kq is the quenching constant and [Q] is the quencher concentration. Kq is the slope obtained from the plot of I_0/I vs [Q].

Viscosity Measurement

In order to further investigate the mode of interaction between binding of metal complexes (1–4) with CT-DNA, viscosity experiments were carried on an Ostwald viscometer immersed in a thermostatic water bath maintained at 303±0.1 K. Titrations were performed for complexes (1–4) by introducing each complex into the DNA solution present in the viscometer. Flow time was measured with a digital stop watch; three times for each sample and an average flow time was calculated. Data were presented as $(\eta/\eta_0)^{1/3}$ versus binding ratio [37].

DNA Photo Cleavage

The cleavage studies of supercoiled pBR 322 DNA (50 μM) was carried out in the agarose gel electrophoresis instrument.

Table 4 Activation parameters for the formation of copper (II) complex

Cu(II) complex Temp (K)	ΔG* (kJ $mole^{-1}$)	Equation and R^2	ΔH* (kJ mol^{-1})	ΔS* (kJ K^{-1} mol^{-1})
288	79.11			
298	81.51	y=221.5x+15369	15.37	−0.221
303	82.51	R^2=0.997		
308	83.54			

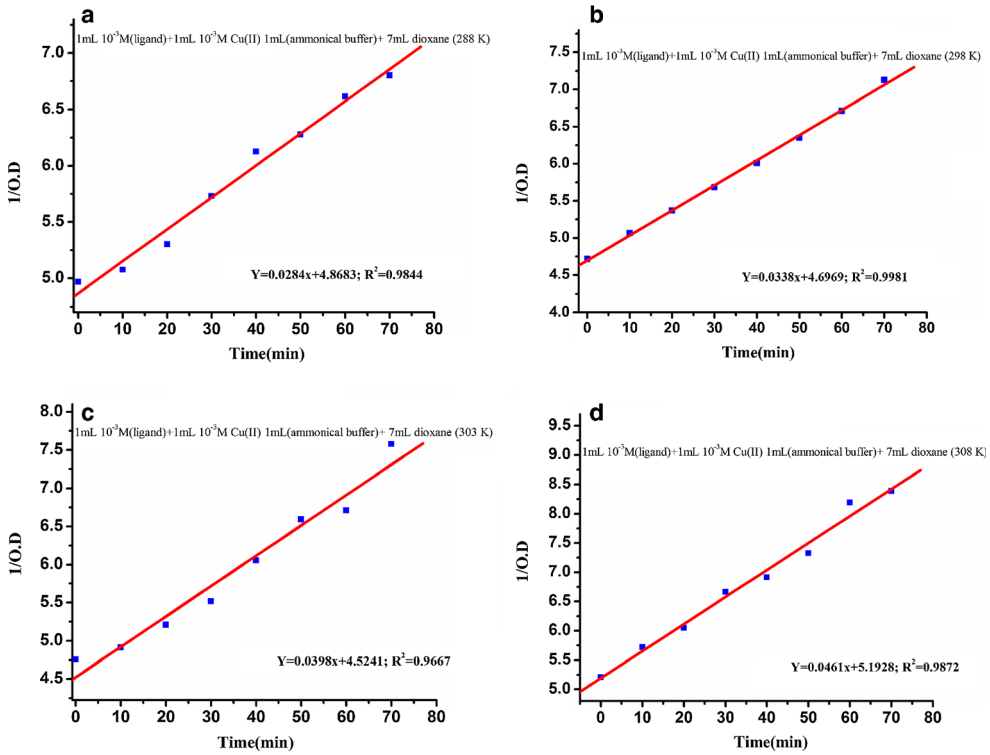

Fig. 3 Second order graphs of Cu (II)-3-MBTMPD complex at different temperatures (288, 298, 303 and 308 K)

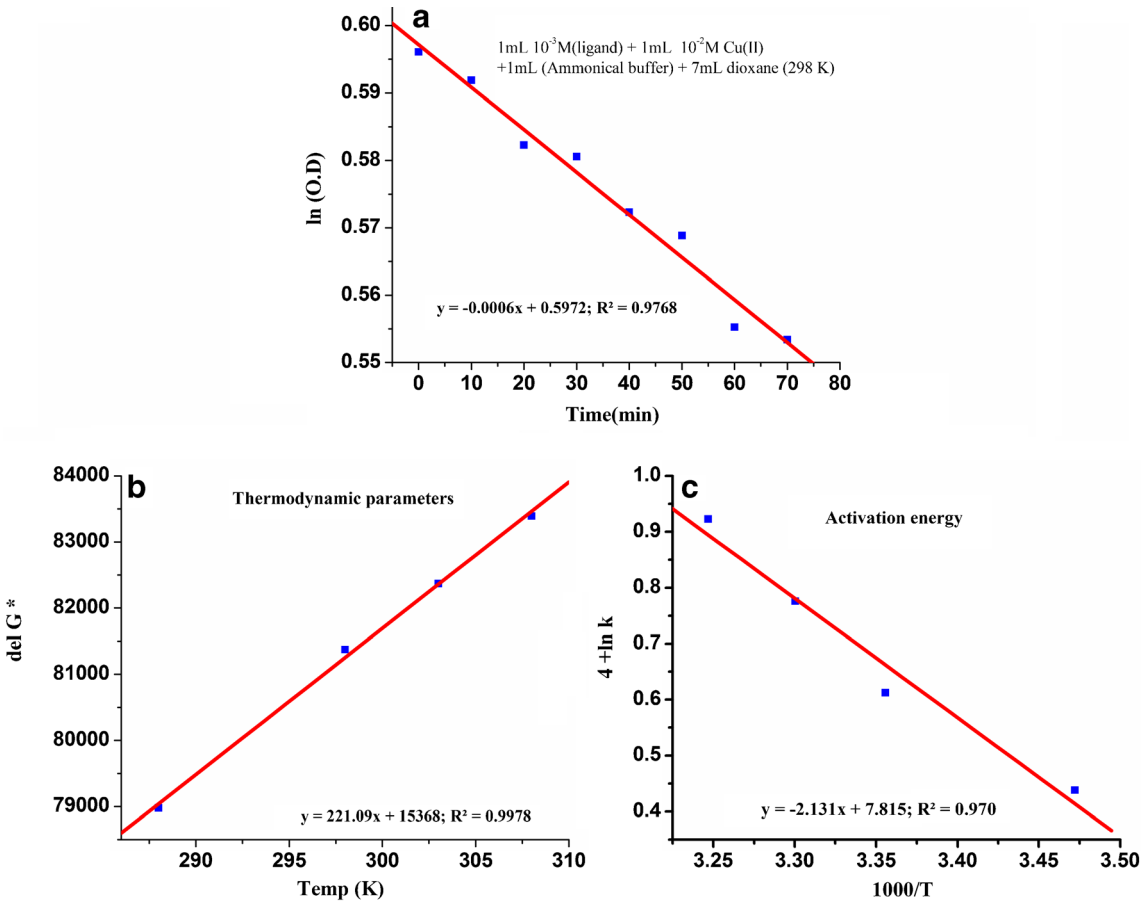

Fig. 4 **a** First order graph, **b** Thermodynamic parameter graph, **c** Activation energy graph of Cu (II)-3-MBTMPD

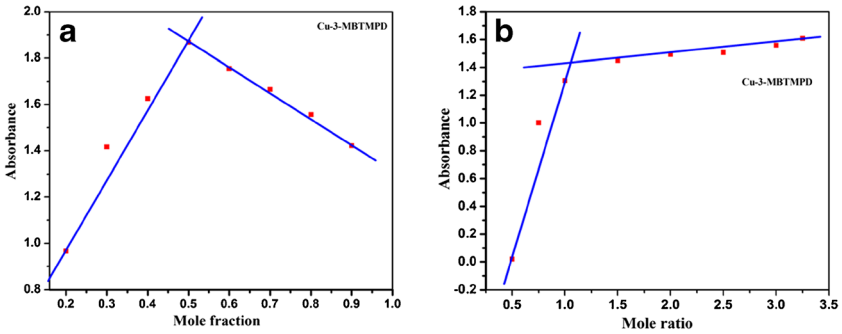

Fig. 5 Plots of Cu (II)-3-MBTMPD. **a** Job's method and **b** Mole ratio method

Here supercoiled pBR322 DNA (1 μL) was treated with the metal complexes (1-4) in buffer (Tris-HCl, 18 mmole NaCl; pH: 7.2) and the solution was then irradiated at room temperature with a UV Lamp (365 nm) for 30 min. After that the sample was mixed with loading buffer (3 μL) containing 25 % bromophenol blue, 0.25 % xylene cyanol and 30 % glycerol (2 μL). The samples were subjected to electrophoresis for 1 h at 50–100 eV on 1 % agarose gel using Tris-acetic acid EDTA buffer (pH: 7.2). The gel was then stained using 1 mg /1 mL ethidium bromide (EB) [42]. The gel was viewed with documentation system and photographed using a CCD camera (Bio-Rod).

Antibacterial Activity

The disc diffusion method [43, 44] was used to check the antibacterial activity of the synthesized compounds against four bacterial strains viz; Staphylococcus aureus, Bacillus subtilis, Escherichia coli and Pseudomonas putida. Each organism was cultured in nutrient broth at 310 K for 24 h. Then 1 % broth culture containing approximately 10^6 colony-forming units (CFU/mL) of test strain was added to nutrient agar medium at 318 K and poured into sterile petri plates. The medium was allowed to solidify. 5 μL of the test compound (40 mg/mL in DMSO) was poured on 4 mm sterile paper discs and placed on nutrient agar plates. In each plate standard antibacterial drug (ampicillin) and metal complexes were added. The plates were incubated at 310 K for 24 h and the antibacterial activity was determined by measuring the diameter of zones showing complete inhibition (mm).

Cytotoxicity

The Cytotoxic effect of (1–4) complexes was carried out using a standard MTT assay [45]. The samples (1–4) to be tested were dissolved in DMSO in the concentration range of 1–100 μM. Cells were seeded in a 96-well plate and kept in 5 % CO_2 attachment and grown for 48 h. Then the cells were treated with various concentrations of the complex dissolved in DMSO and incubated for 24 h. After completion of incubation the culture medium was removed and 15 μL of the MTT dye solution (5 mg/ml in phosphate-buffered saline) (PBS) was added to each well and incubated for 4 h. After 4 h incubation in dark, MTT was discarded and DMSO (100 μL/well) was added to solubilize the purple product. The absorbance at 620 nm in each well was measured with a Elisa reader (Thermo Scientific Multi Scan EX) by keeping medium without complex as control. The IC_{50} values were calculated from the plotted absorbance data of the dose response curves.

Molecular Docking

Docking is a method which predicts the preferred orientation of one molecule to another molecule when bound together to

Table 5 Data showing the mole fraction of ligand and absorbance values of Cu (II) and 3-MBTMPD system in dioxane medium at 303 K

Sl. No	Cu (II) Solution (mL)	3-MBTMPD Solution (mL)	Buffer (mL)	Total Volume (mL)	Mole fraction	Absorbance (Abs)
1.	2	18	5	25	0.9	1.4213
2.	4	16	5	25	0.8	1.5568
3.	6	14	5	25	0.7	1.6651
4.	8	12	5	25	0.6	1.7547
5.	10	10	5	25	0.5	1.8683
6.	12	8	5	25	0.4	1.6251
7.	14	6	5	25	0.3	1.4168
8.	16	4	5	25	0.2	0.9666

Table 6 Data showing the mole ratio of ligand and absorbance values of Cu^{II} and 3-MBTMPD system in dioxane medium at 303 K

S.No.	Cu^{II} Solution (mL)	3-MBTMPD Solution (mL)	Buffer (mL)	Concentration of metal	Concentration of ligand	Moleratio [L] /[M]	Absorbance (Abs)
1.	4	2	5	16×10^{-5}	8×10^{-5}	0.5	1.001
2.	4	3	5	16×10^{-5}	12×10^{-5}	0.75	1.305
3.	4	4	5	16×10^{-5}	16×10^{-5}	1	1.448
4.	4	6	5	16×10^{-5}	24×10^{-5}	1.5	1.493
5.	4	8	5	16×10^{-5}	32×10^{-5}	2	1.506
6.	4	10	5	16×10^{-5}	40×10^{-5}	2.5	1.557
7.	4	12	5	16×10^{-5}	48×10^{-5}	3	1.608
8.	4	13	5	16×10^{-5}	52×10^{-5}	3.25	1.650

form a stable complex. There are many types of software viz; Gold [46]. Flex, Glide and Autodock available to study Receptor-Guest and Receptor-Receptor interactions. In the present investigation, Gold software was employed to identify the Receptor- Guest molecule interactions.

Results and Discussion

FT-IR

In IR spectrum of title compound the peak observed at 3363 cm^{-1} corresponds to νO-H, band at 1633 cm^{-1} corresponds to νC=N and the peak at 1220 cm^{-1} indicates the presence of phenolic νC-O. A comparison of IR spectra of metal complexes with title compound reveals decrease in stretching frequency of νC=N, νC-O of phenolic group, and the disappearance of νO-H frequency in metal complexes indicating the participation of oxygen and nitrogen atoms in bonding. In the spectra of metal complexes new bands appeared at 680–540 cm^{-1} and 462–397 cm^{-1} [47] correspond to νO-M and νN-M respectively. One broad band appeared in the region 3552–3358 cm^{-1} corresponds to νO–H vibrations indicating the presence of coordinated water molecules in all the complexes [48].

UV-Visible

UV-Vis absorption spectroscopic technique can help to evaluate the geometry of metal complexes Fig. 1. The UV–Visible

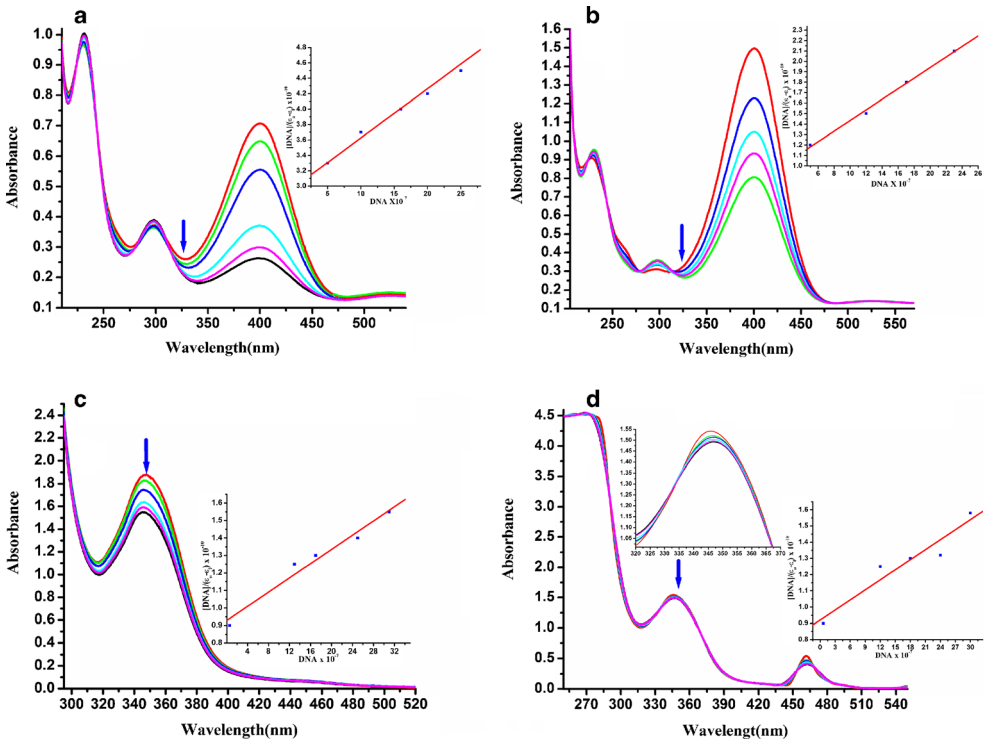

Fig. 6 Absorption spectra of complexes (**a**) Cu (II), (**b**) Cd (II), (**c**) Ce (IV), and (**d**) Zr (IV) in Tris-HCl buffer by addition of CT-DNA. Arrow shows the hypochromic and bathochromic shift upon increase of the DNA concentration. Plots of [DNA]/($\varepsilon_a - \varepsilon_f$) vs [DNA] for the titration of DNA with Imine base metal complexes

Table 7 Absorption and quenching constants of imine base complexes

Compound	Absorption constant (K_b)	quenching (K_q) constant
Cd-3-MBTMPD	3.3×10^5	3.5×10^5
Cu-3-MBTMPD	5.5×10^5	5.1×10^5
Zr-3-MBTMPD	1×10^5	1.15×10^5
Ce-3-MBTMPD	1.25×10^5	1.3×10^5

spectrum of title compound displayed bands at 223 nm, 273 nm and 352 nm. These bands are attributed to π→π* transitions arising from the benzene ring and the double bonds of the azomethine (N=C) group [10] and n→π* transition arising from non-bonding electrons present on the nitrogen of the azomethine group. The electronic spectrum of Cu (II) complex exhibits bands at 226 nm, 326 nm are attributable to charge transfer transitions, while the peaks at 410 nm and 567 nm are assignable to spin-allowed and laporte forbidden but vibronically allowed d-d transitions viz; $^2B_{1g}\rightarrow{}^2A_{1g}$, and $^2B_{1g}\rightarrow{}^2E_g$. The magnetic susceptibility in the solid state shows that the copper complex is paramagnetic with magnetic moment (1.8 B.M.) in the range normally found for square-planar copper complexes. The proposed structures of the complexes are given in Fig. 1. The electronic spectrum of Zr (IV) complex exhibited very weak bands. In Ce (IV) complex bands at 280 nm, 347 nm, and in Cd (II) complex at 230 nm and 297 nm are assignable to charge transfer transitions.

SEM and EDX

The ligand and its 1:1 metal complexes showed different surface morphologies. The SEM images of 3-MBTMPD showed elongated flakes. The EDX method was employed to analyze the elements present on the surface of the compounds. The SEM images of complexes presented in Fig. 2 correspond to Cu (II)-3-MBTMPD complex with the morphology of irregular small rock like appearance in their shape and Cd (II)-3-MBTMPD with grassy spindle like appearance. While Ce -3-MBTMPD (IV) and Zr (IV)-3-MBTMPD displayed irregular cluster of particles.

Kinetic Studies

The experiment is carried out under (i) Pseudo first order reaction condition (1 mL 10^{-3} M (ligand)+1 mL 10^{-2} M Cu (II) +1 mL ethanolic ammonia buffer+7 mL dioxane) at 298 K and (ii) second order reaction condition (1 mL 10^{-3} M (ligand)+1 mL 10^{-3} M Cu (II) ion +1 mL ethonalic ammonia buffer+7 ml dioxane at four different temperatures (288 K, 298 K, 303 K and 308 K).

The reaction was performed in dioxane medium under pseudo condition by maintaining a large excess of metal ion over the imine base ligand. To the above reaction mixture 1 mL of ethanolic buffer was added towards maintaining the pH at 7–8. The progress of the reaction was monitored at regular intervals of time using spectrophotometer. Plots of ln (O.D) vs time have been found to be linear with negative slope indicating first order with

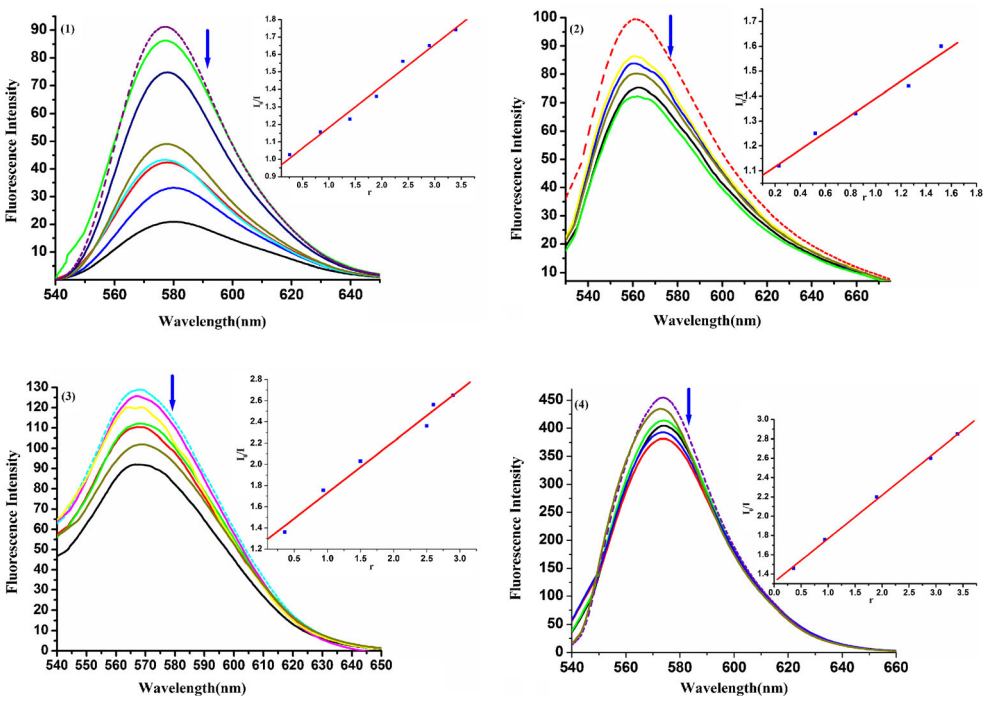

Fig. 7 Emission spectra of the DNA–ethidium bromide (EB) system (1) Cu(II), (2) Cd(II), (3) Ce(IV) and (4) Zr(IV). *Arrows* show the emission intensity changes upon increasing concentration of the compounds. Insert: Stern–Volmer fluorescence quenching plots

respect to concentration of ligand. However, under equimolar conditions ([Ligand]=[Metal ion]), the plots of reciprocal of absorbance vs. time have been found to be linear with positive slopes and an intercept on the ordinate indicating the overall reaction as second-order.

Activation parameters for these reactions are computed from Eyring's plot and the data for the evaluation of second-order rate constants at various temperatures are compiled in Tables 1, 2, 3 and 4. The formation of metal complex of candidate imine base was conducted at four different temperatures viz. 288, 298, 303 and 308 K. The rate constant increased substantially with increase in temperature. Activation energy (E_a) is calculated using Arrhenius plot Figs. 3 and 4. ΔG^* values for four different temperatures are calculated following Eyring equation.

$$K = (RT/Nh)\exp(-\Delta G^*/RT)$$

$$\Rightarrow \Delta G^* = -RT \ln(KNh/RT)$$

Where R, N, h and T represent the Gas constant, Avogadro number, Planck's constant and reaction temperature respectively. Thermodynamic parameters such as ΔS^* and ΔH^* were evaluated from Gibbs-Helmholtz equation.

$$\Delta G^* = \Delta H^* - T\Delta S^*$$

Plot of ΔG^* versus T were found to be linear with positive slope. Intercept is equal to ΔH^* and slope corresponds to ΔS^*. Rate constants, activation energy and thermodynamic parameters of Cu (II)-3-MBTMPD are given in Table 4.

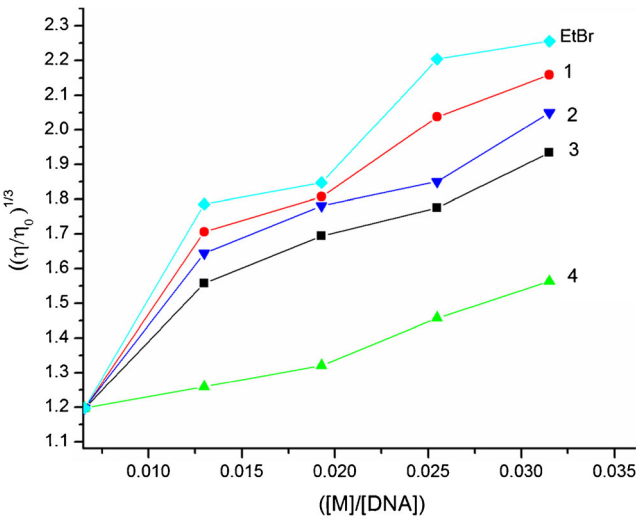

Fig. 8 Effect of increasing amount of ethidium bromide, (1) Cu(II)-3-MBTMPD, (2) Cd (II)-3-MBTMPD, (3) Ce (IV)-3-MBTMPD, (4) Zr (IV)-3-MBTMPD, on relative viscosity of CT-DNA at 300±0.1 K

Stoichiometry Studies

Job's Continuous Variation Method

The solutions of the Cu (II) and 3–MBTMPD with same molar concentrations (0.00125 M) are mixed in varying volume ratios, keeping the total volume of the mixture constant. The pH of the sample solutions were maintained constant by the addition of a buffer solution consisting 3 mL of sodium acetate buffer. The absorbance of each sample is measured at 412 nm. The plot of absorbance against mole fraction of ligand showed maximum absorbance at 0.50 mole fraction Fig. 5. The calculated mole fraction values and absorbance are given in Table 5.

Mole-Ratio Method

A series of solutions of constant volume were prepared keeping the molar concentration of the metal Cu (II) constant in respective systems and varying the concentration of 3 – MBTMPD. The pH of these samples were maintained constant with the

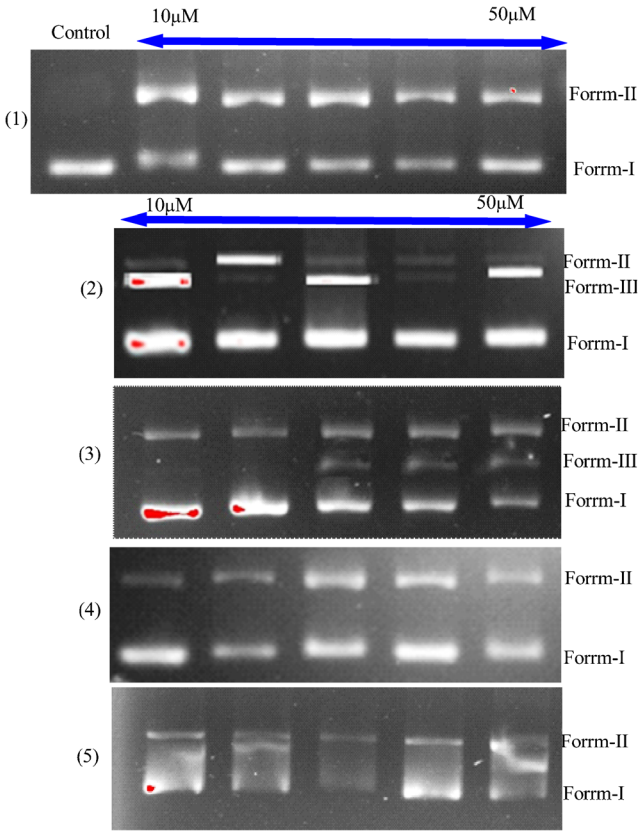

Fig. 9 Photo cleavage studies of pBR322 DNA, in the absence and presence of complexes (1) [Ce (IV)-3-MBTMPD], (2) [Cd (II)-3-MBTMPD], (3) [Cu (II)-3-MBTMPD] and (4) [Zr (IV)-3-MBTMPD] and (5) [3-MBTMPD]. 30 min irradiation at 365 nm. *Lane* 0 control plasmid DNA (untreated pBR322), five sets of 5 *lanes with* 10 μM, 20 μM, 30 μM, 40 μM and 50 μM respectively

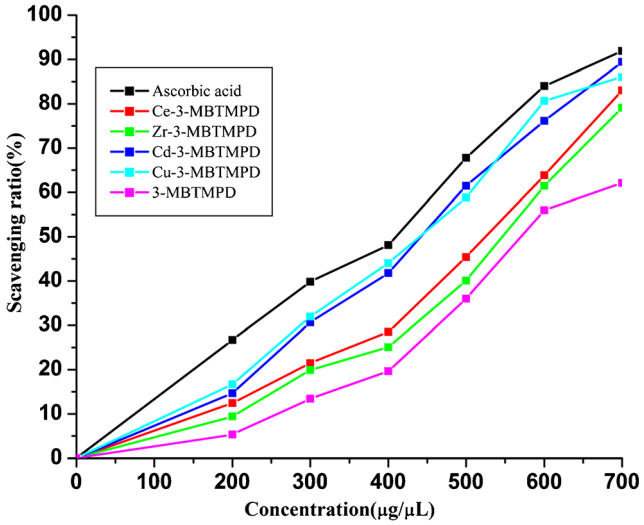

Fig. 10 Radical-scavenging activity of the synthesized compounds on DPPH radicals (%)

help of the acetate buffer. Data of absorbance versus concentration of ligand to metal is given in Table 6. The plot of the absorbance versus mole ratio ([ligand] /[Metal]) corresponds to 1 : 1 composition of Cu(II)-3-MBTMPD Fig. 5.

DNA Binding Studies

The binding abilities of metal complexes with CT-DNA via intercalation mode have been explored in the present investigation. In the intercalative mode of binding, the π* orbital of the intercalated ligand couple with the π orbital of the DNA base pairs decreasing in π – π* transition energy and resulting in bathochromism [49, 50] and a significant hypochromism [51], suggesting that the complexes used in this study have strong binding interaction with DNA in an intercalative mode Fig. 6. In order to determine the intrinsic binding strength of (1–4) metal complexes the K_b values Table 7 were calculated using the Eq. (1). The K_b values of Cu(II) 3-MBTMPD (5.5×10^5 M^{-1}), Cd (II) 3-MBTMPD (3.3×10^5 M^{-1}), Ce (IV) 3-MBTMPD (1.25×10^5 M^{-1}) and Zr (IV) 3-MBTMPD (1×10^5 M^{-1}) indicate order of binding affinities as; Cu(II) > Cd(II) > Ce(IV) > Zr(IV).

Quenching Studies

To further characterize the exact nature of the binding mode of metal complexes with DNA, ethidium bromide (EB) displacement assay, an experiment based on emission titration has been widely used. It was previously reported that the enhanced fluorescence can be quenched by the addition of a second molecule. In our experiment as depicted in Fig. 7, for complexes 1, 2, 3 and 4 the fluorescence intensity of EB at 584 nm showed a remarkable decreasing trend with the increasing concentration of the complex and is due to displacement of the DNA bound EB by metal complex. The Kq values were calculated from Stern- volmer equation and are in the order of 5.1×10^5 M^{-1} Cu (II)>3.5×10^5 M^{-1} Cd (II) >1.3×10^5 M^{-1} Ce (IV)>1.15×10^5 M^{-1} Zr (IV) (Table 7).

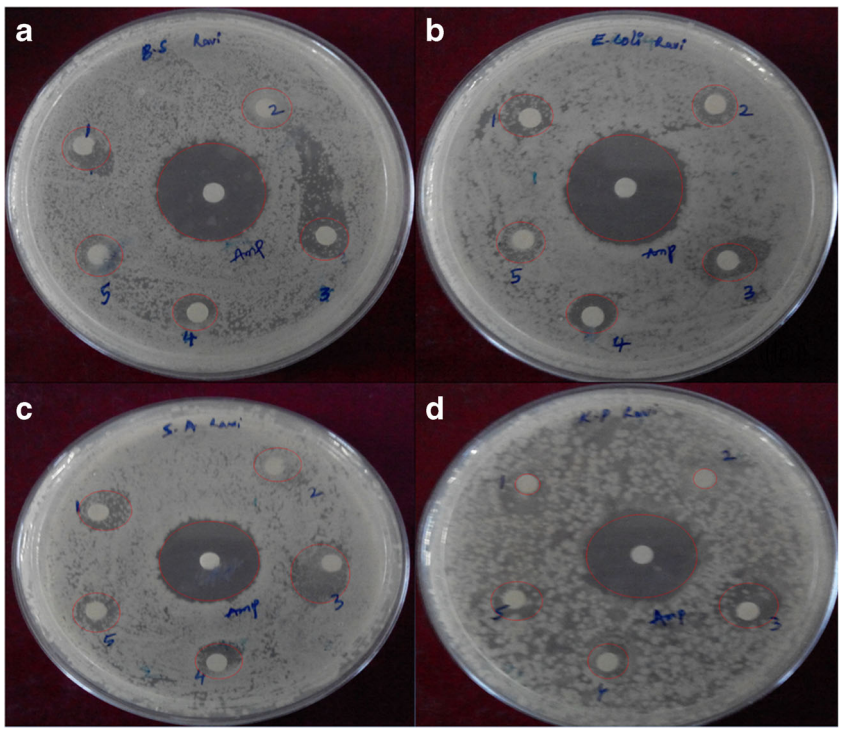

Fig. 11 Antimicrobial activity of Cu(II)-3-MBTMPD, Cd(II)-3-MBTMPD, Ce(IV)-3-MBTMPD, Zr(IV)-3-MBTMPD and 3-MBTMPD (**a**) B.subtilis, (**b**) E.coli, (Gram Negative) (**c**) S. areus and (**d**) K. Pneumonia bacteria, (Gram Positive) ampicillin as positive control

Table 8 Minimum inhibition zone(mm) of complexes (μg/mL)

Compound	Bacterial inhibition zone (mm)		Bacterial inhibition zone (mm)	
	Gram (+)		Gram (−)	
	B.subtilis	S. areus	K. Pneumonia	E.coli
3-MBTMPD	7	8	5	6
Cd-3-MBTMPD	10	14	10	10
Cu-3-MBTMPD	7	9	8	9
Zr-3-MBTMPD	8	10	5	8
Ce-3-MBTMPD	10	10	6	8
Ampicillin	18	25	25	21

Viscosity Measurements

To further provide the proof of binding mode of (1–4) metal complexes with CT-DNA, viscosity measurements [37] were carried by keeping DNA concentration constant (5 μM) and increasing concentration of metal complex in respective systems (Fig. 8). In general classical intercalation model predicts in lengthening of DNA helix, as base pairs are pushed apart to accommodate the bound complexes leading to the increase in viscosity of DNA. In present investigation, the representative profile of comparative viscosity measurements for binding nature of (1–4) metal complexes with CT-DNA are informative in predicting intercalative mode of binding as there is rise in viscocity with increase of metel complex concentration in all the systems. The comparison of relative viscosities of (1–4) metal complexes and ethidium bromide (EB) showed the binding affinity order as; EB >1>2>3>4.

DNA Photo Cleavage Studies

The cleavage studies of plasmid DNA induced by (1–4) metal complexes were monitored by agarose gel electrophoresis Fig. 9. When plasmid DNA is subjected to electrophoresis, fast movement is observed for the intact supercoiled form (form I). If scissoring occurs on one strand, the supercoiled form will relax to generate a slower-moving open circular form (form II). If both strands are cleaved, a linear form (Form III) will be generated in between form I and Form II [49, 50, 52]. The pBR322 DNA was incubated with different concentrations of complexes (1–4) and irradiated at 365 nm for 30 min. As the concentration of complexes (1-4) is increased from 10 to 50 μM, the percentage of supercoiled (form I) decreased, whereas the amount of form II increased and form III observed significantly. From the graph it is clear that Cu (II) complex exhibited more photo cleavage activity compared to other complexes.

Antioxidant Properties

The model of scavenging the stable DPPH radical is a widely used technique to screen antioxidant properties by spectrophotometer in a very short time period. When the reaction between antioxidant molecule and DPPH radical [53] occurs, it results in decrease in absorbance at 517 nm. This is because the radical is scavenged by antioxidants through donation of hydrogen to form the reduced form (DPPH-H), and this property is also visually noticeable as the color changes from purple to yellow. The more rapidly the absorbance decreases, the more potent is the antioxidant compound. In the present study the antioxidant activity of 3-MBTMPD and its metal complexes was evaluated by scavenging stable DPPH radical

Table 9 Cell viability values (%) of the lignad and metal (II) and (IV) complexes against selected cell lines

	% of cell viability					
	HeLa			MCF-7		
Compound	10 μM	20 μM	30 μM	10 μM	20 μM	30 μM
3-MBTMPD	90 %	87 %	69 %	88 %	79 %	57 %
Cu-3 MBTMPD	78 %	48 %	31 %	65 %	55 %	28 %
Cd-3 MBTMPD	79 %	54 %	39 %	75 %	60 %	30 %
Ce-3 MBTMPD	89 %	74 %	52 %	86 %	64 %	47 %
Zr-3 MBTMPD	84 %	62 %	49 %	81 %	50 %	38 %

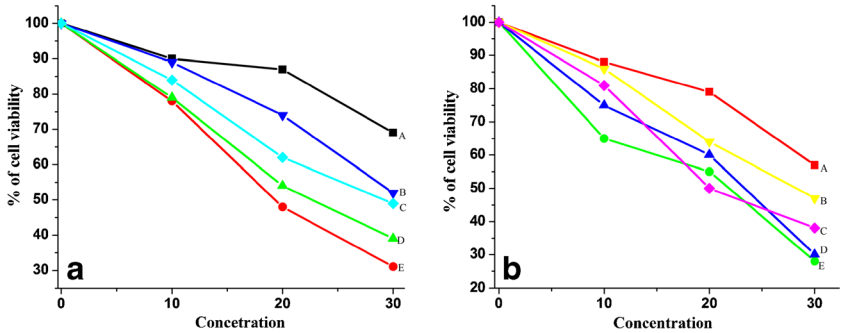

Fig. 12 Effect of A–E on cell viability and growth: (**a**) HeLa and (**b**) MCF-7 cells were treated with different concentrations of the test compound for 36 h and then the cell viability was measured by the MTT assay. (*A*) 3-MBTMPD, (*B*) Zr(IV)-3-MBTMPD (*C*) Ce(IV)-3-MBTMPD, (*D*) Cd(II)-3-MBTMPD, (*E*) Cu(II)-3-MBTMPD, in HeLa and in MCF-7 cells

(Fig. 10). The DPPH radical scavenging activities were found to be 26.74 % for ascorbic acid, 16.76 % for Cu (II)-MBTMPD, 14.7 % for Ce(IV)- MBTMPD, 12.26 % for Cd(II))- MBTMPD, 9.46 % for Zr(IV)- MBTMPD, and 5.34 % for 3-MBTMPD, at concentration of the 200 μg μL^{-1}. Ascorbic acid exhibited higher DPPH scavenging activity than the compounds at all the concentrations. At the concentration of 700 μg μL^{-1},

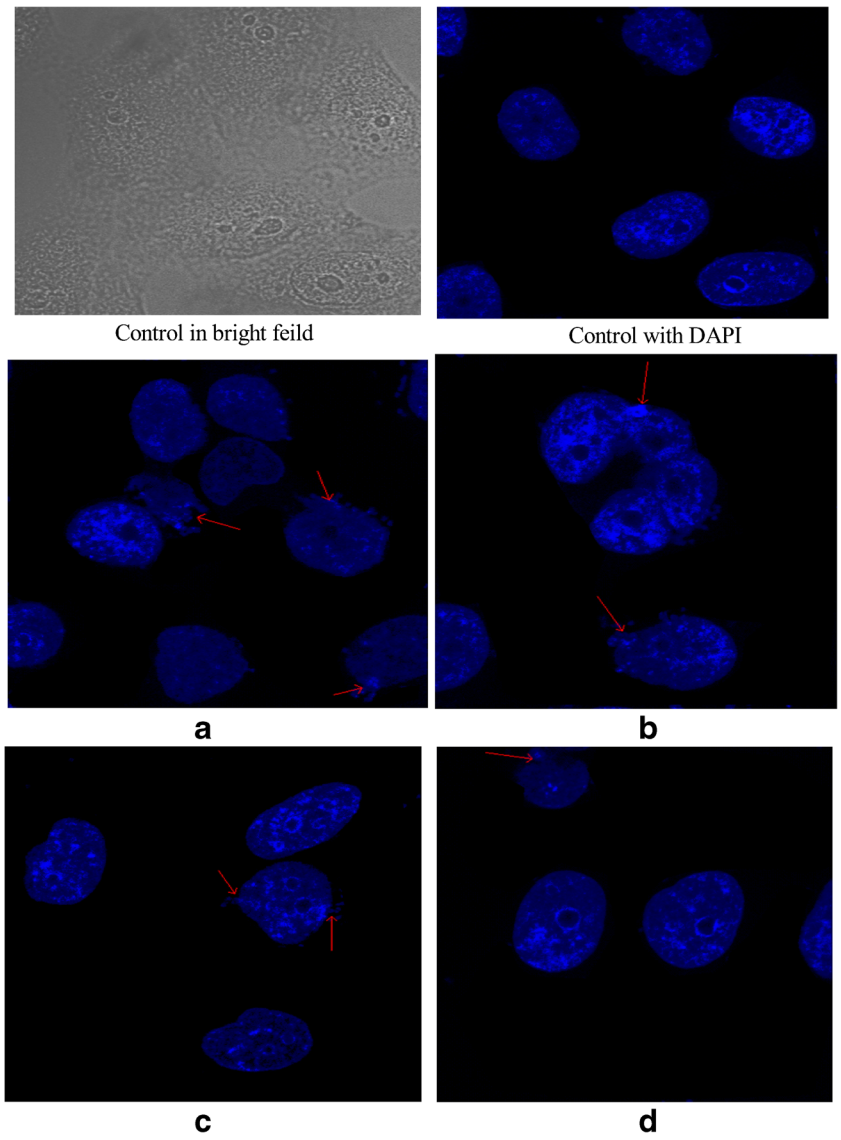

Fig. 13 Confocal images of HeLa cells stained with four complexes. Control (untreated cells) with DAPI stained and bright filed images. Cells were incubated with 20 mM complexes (**a**-1), (**b**-2), (**c**-3) and (**d**-4) and observed by confocal microscopy (excitation, 488 nm; emission, 600–620 (nm). Blebbing of the nuclei is clearly observed

scavenging activities were found to be 91.85, 86.09, 89.44, 83, 79.12 and 62.12 % for Ascorbic acid, Ce (IV)-MBTMPD, Cu (II)-MBTMPD, Cd(II)- MBTMPD, Zr(IV)- MBTMPD and 3-MBTMPD respectively.

The metal scavenging activity which is the measure of antioxidant property at the concentration of above compounds at 200 μg μL^{-1} follows the order: Ascorbic acid> Cu (II)-MBTMPD >Ce (IV)- MBTMPD >Cd(II)- MBTMPD > Zr(IV)- MBTMPD.>3-MBTMPD while at higher concentration the same order is followed except that Cu(II) and Ce (IV) complexes exchanged their position.

Anti- Bacterial Studies

The antibacterial screening of the ligand (3-MBTMPD) and its (1–4) metal complexes were performed against gram positive (B. Subtilis and S. Aureus) and gram negative bacteria (E. Coli and K. Pneumonia) by the disk diffusion method [54]. The activities of the compounds were compared with standard Ampicillin for antibacterial activity. The antibacterial properties of the imine base and its metal complexes evaluated and presented in Fig. 11 and Table 8, indicate that the compounds are active in exhibiting antibacterial role. The order of activity towards gram negative bacteria is: Cd (II)-3-MBTMPD >Ce (IV)-3-MBTMPD> Zr (IV) -3-MBTMPD> Cu (II)-3-MBTMPD > 3-MBTMPD and for gram positive bacteria the order is Cd (II)-3-MBTMPD> Cu (II)-3-MBTMPD> Ce (IV)-3-MBTMPD> Zr (IV)-3-MBTMPD> 3-MBTMPD.

Cytotoxic Assay In-Vitro

Cytotoxic studies evaluated by using MTT assay, HeLa(Human cervical cancer cell line) and MCF-7 (breast cancer cell line) tumor cell lines were treated with different concentrations (10, 20, and 30 μM) of metal complexes. The increase of number of abnormal cells with increase in concentration of compounds reveals the concentration effect of studied compounds (Table 9 and Fig. 12) on cytological changes [45]. Cell death is studied by treating the HeLa cancer cells with 20 μM of 1–4 for 24 h and then observing them for cytological changes by adopting DAPI staining. The representative morphological changes observed for metal complexes (1–4) such as nuclear swelling, cytoplasmic blebbing and late apoptosis indication of dot-like chromatin condensation are shown in Fig. 13. The results of current investigation predict the order for apoptosis-inducing effect as; Cu (II) 3-MBTMPD > Cd (II) 3-MBTMPD> Ce (IV) 3-MBTMPD> Zr (IV) 3-MBTMPD> 3-MBTMPD. The IC_{50} value of all the compounds in present study vary from 1 to 3 μM (Table 10) and indicate that they have relatively high antitumor activity than free ligand 3-MBTMPD.

Table 10 The IC_{50} values for complexes against HeLa and MCF-7 cell lines

Compound	IC_{50}	
	HeLa	MCF-7
3-MBTMPD	70±1.2 μM	65.66±1.5 μM
Cu-3 MBTMPD	38.33±1.8 μM	32.33±1.7 μM
Cd-3 MBTMPD	45.33±2.1 μM	39±0.9 μM
Ce-3 MBTMPD	50±1.2 μM	45.66±1.5 μM
Zr-3 MBTMPD	56.33±1.8 μM	54.33±1.7 μM

Molecular Modeling and Docking

The protein crystal structure 2OIQ.pdb (proto-oncogene tyrosine-protein kinase src) was downloaded from the PDB database. The molecule of candidate imine base was built using Chemdraw software [55, 56]. Later it was minimized using steepest descent and followed by conjugate gradient and energy minimization stabilized at 110811.0 Kcal mol^{-1}. After preparation of receptor the docking was carried out with GOLD software. The results obtained were analyzed and highest dock score values were taken and hydrogen bond interactions of receptor with imine base and metal complexes in respective systems have been explored. The corresponding data were measured and tabulated in Table 11. The ligand molecule was bound with the receptor of 2OIQ.pdb as shown in Figs. 14 and 15. The binding interactions are found at the cavity of Proline 485 H_β with Ligand O_{21} with H-bond distance is 2.22A°. The hydrogen bond interaction shown with dotted lines with their partners and amino acid residues were labeled as shown in Fig. 14.

Table 11 Binding of amino acid receptors and hydrogen bonding interactions (A) 3-MBTMPD (B) Cd (II) 3-MBTMPD

Amino acid in the Receptor	Binding site of Reseptor	H- bonding interactions (A°)
A		
Glu-476H_A	O_{19}	3.67
Glu-476H_{B1}	O_{19}	2.78
Glu-476HO_{E2}	O_{15}	3.43
Lys295NH	O_{29}	2.10
B		
Proline485 Hβ	O_{21}	2.22
Proline485H_2	O_{29}	3.52
Proline482 Hg_2	O_{28}	3.91
Proline482 Hg_2	O_{28}	3.65
Arginine460Nb_1	O_{22}	2.91

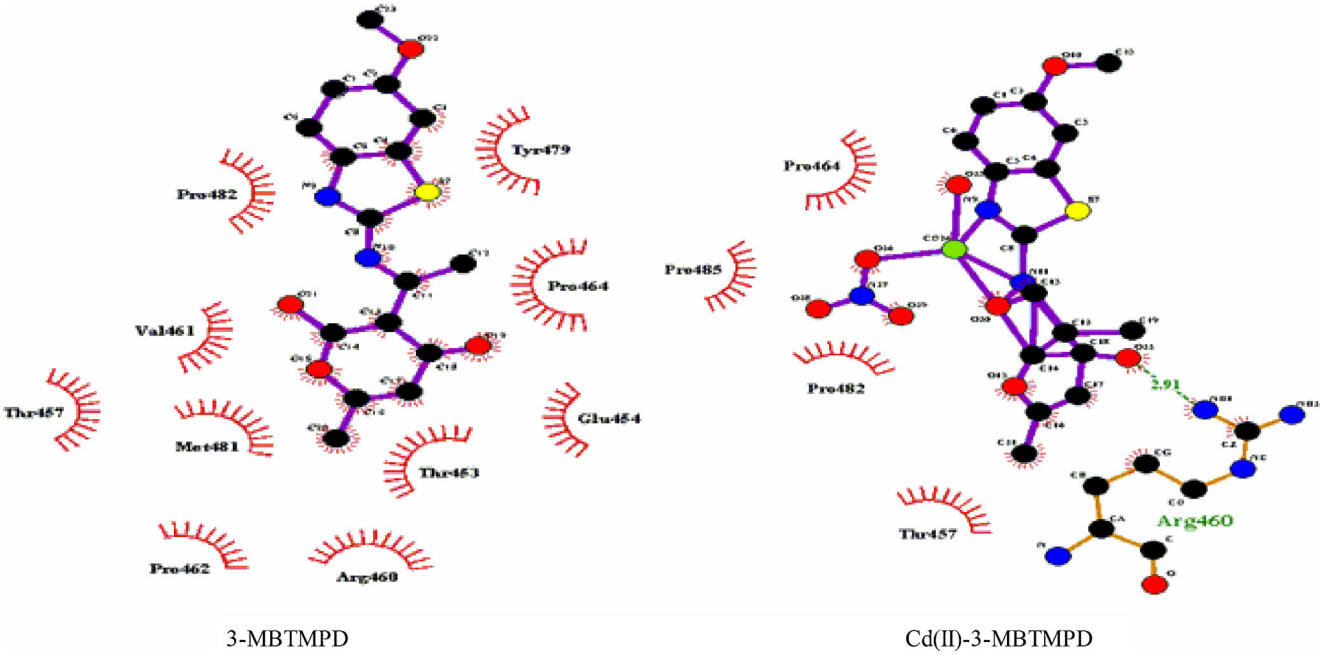

Fig. 14 Hydrogen bonds and hydrophobic contacts of 3-MBTMPD and Cd (II)-3-MBTMPD

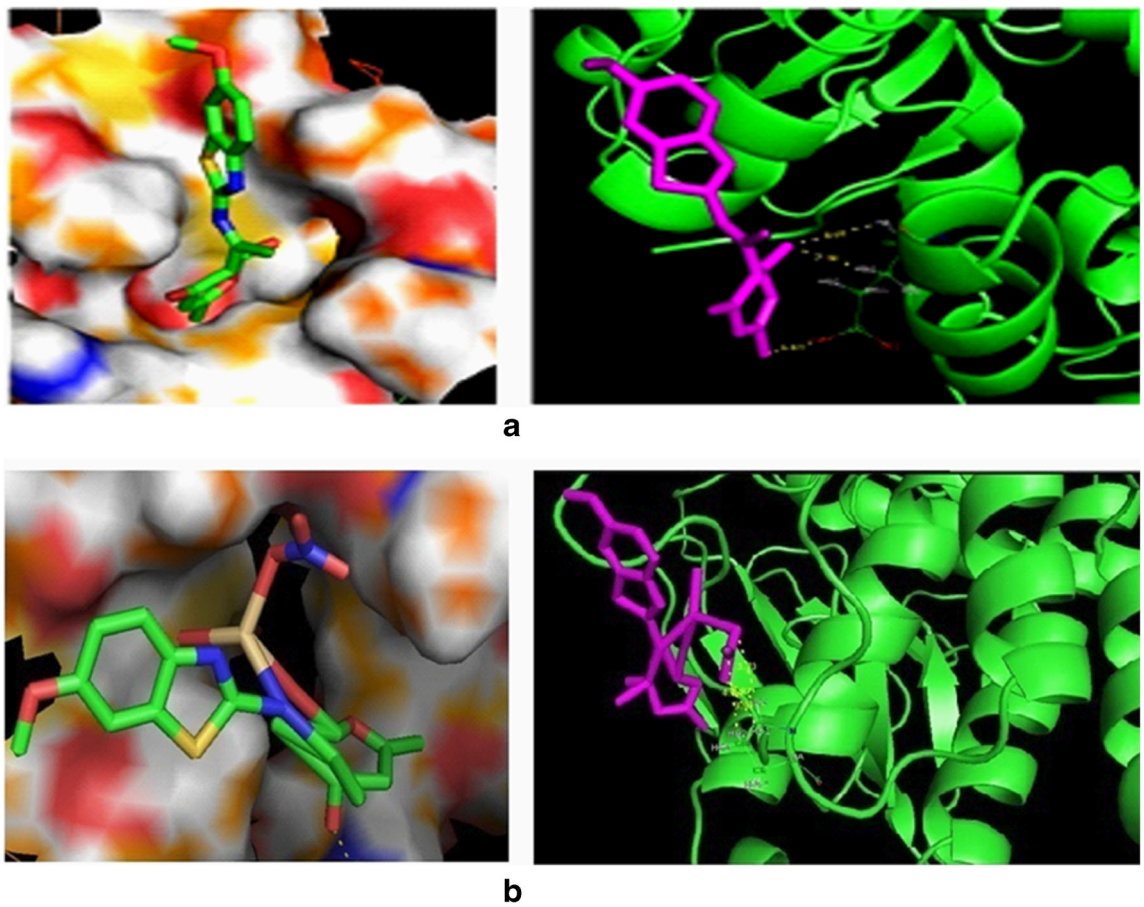

Fig. 15 **a** (i) Surface representation of receptors and (ii) H-bonding interactions in 3-MBTMPD. **b** (i) Surface representation of receptors and (ii) H-bonding interactions in Cd (II)-3-MBTMPD

Conclusions

The geometry of metal complexes of Cu (II), Cd (II), Ce (IV) and Zr (IV) were found to be square planar, tetrahedral, octahedral and square pyramidal respectively. Surface morphology studies of these metal complexes were carried out with the help of scanning electron microscope (SEM). Copper complex showed an irregular small rock-like structure, cadmium complex showed grassy spindle-like structure, Ce (IV) and Zr (IV) showed varying size of irregular clusters of particles. The kinetic studies revealed that the reaction is of first-order with respect to ligand and under equimolecular conditions the overall reaction is of second-order. DNA binding studies of Cu (II), Cd (II), Ce (IV) and Zr (IV) complexes were carried out in detail by electronic absorption titration, steady state quenching, viscosity measurements and DNA cleavage by electrophoresis. The results suggest that all the metal complexes bind to CT- DNA through intercalation mode. The antioxidant activity evaluated for the metal complexes have excellent potential drug activity to eliminate the hydroxyl radicals. These observations can lead to the development of new potent antioxidants. The results obtained from in- vitro antibacterial activity studies tested for metal complexes are informative to predict their considerable activity against culture tested. These metal complexes have relatively high antitumor activity compared to free ligand 3MBTMPD. The molecular modeling and docking studies of these complexes have shown their strong binding affinity with receptor sites of amino acid residues at target site.

Acknowledgments We express our gratefulness to UGC-RGNF-ST-AND-9591 for the financial support extended to one of the author. The authors are thankful to the Department of Chemistry, Osmania University, Hyderabad for providing the research facilities. We acknowledge CFRD and the DBT-ISLARE, Osmania University for facilitating required data acquisition from instrumental studies. Further we are also thankful to National Institute of Nutrition (NIN) and Centre for DNA Fingerprinting and Diagnostics (CDFD) Hyderabad for providing facilities in carrying out cytotoxicity studies.

References

1. Rosenberg B, VanCamp L, Krigas T (1965) Inhibition of Cell Division in Escherichia coli by Electrolysis Products from a Platinum Electrode. Nature 205:698–699
2. Reedijk J (1996) Improved understanding in platinium antitumour chemistry. Chem Commun 801–806. doi:10.1039/CC9960000801
3. Roberts JD, Peroutka J, Beggiolin G, Manzotti C (1999) Comparison of cytotoxicity and cellular accumulation of polynuclear platinum complexes in L1210 murine leukemia cell lines. J Inorg Biochem 77:47–50
4. Jamieson ER, Lippard SJ (1999) Structure, Recognition, and Processing of Cisplatin-DNA Adducts. Chem Rev 99(9):2467–2498
5. Guo ZJ, Sadler PJ (1999) Medicinal inorganic chemistry. Adv Inorg Chem 49:183–306
6. Galanski M, Arion VB, Jakupec MA, Keppler BK (2003) Recent developments in the field of tumor-inhibiting metal complexes. Curr Pharm Des 9(25):2078–2089
7. Tanaka T, Yukawa K, Umesaki N (2005) Combination effects of irradiation and irinotecan on cervical squamous cell carcinoma cells in vitro. Oncol Rep 14:1365–1369
8. Wang D, Lippard S (2005) Cellular processing of platinum anticancer drugs. Nature Rev Drug 4:307–320
9. Berners Price SJ, Appleton TG (2000) In platinum-based drugs in cancer therapy humana press Totowa, N J3:31
10. Angeles Boza AM, Bradley PM, Wicke SE, Bacsa J, Dunbar KM, Turro C (2004) DNA binding and photocleavage in vitro by new dirhodium(II) dppz complexes: Correlation to cytotoxicity and photocytotoxicity. Inorg Chem 43:8510–8519
11. Argyriou AA, Polychronopoulos P, Iconomou G, Chroni E, Kalofonos HP (2008) A review on oxaliplatin-induced peripheral nerve damage. Cancer Treat Rev 34:368–377
12. Li MJ, Lan TY, Lin ZS, Chen CYGN (2013) Synthesis, characterization, and DNA binding of a novel ligand and its Cu(II) complex. J Biol Inorg Chem 18:993–1003
13. More PG, Bhalvankar RB, Patter SC (2001) Synthesis and biological activity of Schiff bases of aminothiazoles. J Ind Chem Soc 78(9):474–475
14. Kabeer AS, Baseer MA, Mote NA (2001) Synthesis and antimicrobial activity of some Schiff bases from benzothiazoles. Asian J Chem 13:496–500
15. Raman N, Joseph J, Velan ASK (2006) Antifungal activities of biorelevant complexes of copper (II) with biosensitive macrocyclic ligands. Mycobiology 34(4):214–218
16. Ma XF, Li DD, Tian JL, Kou YY, Yan SP (2009) DNA binding and cleavage activity of reduced amino-acid Schiff base complexes of cobalt(II), copper(II), and cadmium(II). Trans Met Chem 34:475–481
17. Kozurkova M, Sabolova D, Janovec L, Mikes J, Koval J, Ungvarsky V, Stefanisinova M, Fedorocko P, Kristian P, Imrich J (2008) Cytotoxic activity of proflavine diureas: Synthesis, antitumor, evaluation and DNA binding properties of 1′,1″-(acridin-3,6-diyl)-3′, 3″ dialkyl diureas. Bioorg Med Chem 16:3976–3984
18. Li Y, Yang Z (2010) Rare Earth Complexes with 3-Carbaldehyde Chromone-(Benzoyl) Hydrazone: Synthesis, Characterization, DNA Binding Studies and Antioxidant Activity. J Fluoresc 20:329–342
19. Metcalfe C, Thomas JA (2003) Kinetically inert transition metal complexes that reversibly bind to DNA. Chem Soc Rev 32:215–224
20. Rad FV, Housaindokht MR, Jalal R, Hosseini HE, Doghaei AV, Goghari SS (2014) Spectroscopic and Molecular Modeling Based Approaches to Study on the Binding Behavior of DNA with a Copper (II) Complex. J Fluoresc 24:1225–1234
21. Navarro M, Cisneros Fajardo EJ, Sierralta A, Mestre MF, Silva P, Arrieche D, Marchan E (2003) Design of copper DNA intercalators with leishmanicidal activity. J Biol Inorg Chem 8:401–408
22. Corral E, Hotze ACG, Tooke DM, Spek AL, Reedijk J (2006) Ruthenium polypyridyl Complexes containing the bischelating ligand 2,2′-azobispyridine. Synthesis characterization and crystal structures. Inorg Chim Acta 359:830–838
23. Hotze ACG, Faiz JA, Mourtzis N, Pascu GI, Webber PRA, Clarkson GJ, Kopoulou KY, Pikramenou HMJ (2006) Far-red luminescent ruthenium pyridylimine complexes; building blocks for multinuclear arrays. Dalton Trans 24:3025–3034
24. Ljubijankic N, Zahirovic A, Turkusic E, Kahrovic E (2013) DNA Binding Properties of Two Ruthenium(III) Complexes Containing Schiff Bases Derived from Salicylaldehyde: Spectroscopic and Electrochemical Evidence of CT DNA Intercalation. Croat Chem Acta 86(2):215–222

25. Lerman LS (1961) Structural considerations in the interaction of DNA and acridines. J Mol Biol 3:18–30
26. Sathiyaraj S, Butcher RJ, Balakrishnan CJ (2012) Synthesis, characterization, DN Interaction and in vitro cytotoxicity activities of ruthenium(II) Schiff base complexes. J Mol Strc 1030:95–103
27. Pawlica D, Marszalek M, Mynarczuk G, Sieron L, Eilmes J (2004) New unsymmetrical Schiff base Ni(II) complexes as scaffolds for dendritic and amino acid superstructures. New J Chem 28:1615–1621
28. Abd El-halim HF, Omar MM, Mohamed GG (2011) Synthesis, structural, thermal studies and biological activity of a tridentate Schiff base ligand and their transition metal complexes. Spectrochim Acta- A 78:36–44
29. Senthil Raja D, Bhuvanesh NSP, Natarajan K (2012) Structure–activity relationship study of copper(II) complexes with 2-oxo-1, 2-dihydroquinoline-3-carbaldehyde(4′-methylbenzoyl) hydrazone: synthesis, structures, DNA and protein interaction studies, antioxidative and cytotoxic activity. J Biol Inorg Chem 17:223–237
30. Katta L, Sudarsanam P, Mallesham B, Reddy BM (2012) Preparation of silica supported ceria–lanthana solid solutions useful for synthesis of 4-methylpent-1-ene and dehydroacetic acid. Catal Sci Technol 2:995–1004
31. Park HJ, Kwon JH, Cho TS, Kim JM, Hwang IH, Kim C, Kim S, Kim J, Kim SK (2013) Real-time detectioin of DNA cleavage induced by [M(2,2′ bipyridine)$_2$ (NO_3)](NO_3)(M=Cu(II), Zn(II) and Cd(II)) complexes using linear dichroism technique. J Inorg Bioche 127:46–52
32. Pogozelski WK, Tullius TD (1998) Oxidative Strand Scission of Nucleic Acids: Routes Initiated by Hydrogen Abstraction from the Sugar Moiety. Chem Rev 98(3):1089–1108
33. Macpherson IS, Murphy MEP (2007) Type-II Copper containing enzyme. Cell Mol Life Sci 64:2887–2899
34. Hall DB, Holmlin RE, Barton JK (1996) Oxidative DNA damage through long-range electron transfer. Nature 382:731–735
35. Soliman AA, Linert W (1999) Preparation, characterization and thermal study of new cerium (IV) complexes with the salicylidene -2- aminothiophenol schiff base.Synth. React Inorg Met Org Chem 29(7):1133–1151
36. Venkateswarlu M, Satish Kumar M, Ramgopal S, Kumar UU, Uppalaiah K, Saiprakash PK, Rajanna KC (2011) Kinetics and Mechanism of Certain Acetylation Reactions with Acet amide/Oxychloride in Acetonitrile under VilsmeierHaack Conditions. Helvetica Chimica Acta 94(12):2168–2187
37. Ushaiah B, Shiva Leela D, Ravi M, Anupama B, Perugu S, Gyana Kumari C (2014) Synthesis, characterization, antibacterial, DNA binding and cleavage studies of mixed ligand Cu(II), Co(II) Complexes. J Fluores 24:1687–1699
38. Son WJ, Lin QY, Jiang WJ, Du FY, Qi QY, Wei Q (2015) Synthesis, interaction with DNA and antiproliferative activities of two novel Cu(II) complexes with norcantharidin and benzimidazole derivatives. Spectrochim Acta- A 137:122–128
39. Reichmann ME, Rice SA, Thomas CA, Doty P (1954) A further examination of the mole cular weight and size of deoxypentose nucleic acid. J Am Chem Soc 76:3047–3053
40. Carter MT, Rodriguez M, Bard A (1989) Voltammetric studies of the interaction of metal chelates with DNA. 2. Tris-chelated complexes of cobalt(III) and iron(II) with 1,10 phenan-throline and 2,2′-bipyridine. J Am Chem Soc 111(4):8901–8911
41. Lakowicz JR, Webber G (1973) Quenching of Fluorescence by Oxygen. A Probe for Structural Fluctuations in Macromolecules. Biochemistry 12(21):4161–4170
42. Maitey B, Roy M, Saha S, Chakravarthy AR (2009) Photoinduced DNA and Protein cleavage activity of Ferrocene-Conjugated Ternary Copper(II) Complexes. Organometallics 28(5):1495–1505
43. Kavitha P, Saritha M, Laxma Reddy K (2013) Synthesis, structural characterization, fluorescence, antimicrobial, antioxidant and DNA cleavage studies of Cu(II) complexes of formyl chromone Schiff bases. Spectrochim Acta- A 102:159–168
44. Sirajuddin M, Ali S, Zaib S, Iqbal J, Nawaz Tahir M et al (2015) Design, structural and spectroscopic elucidation and in vitro antimicrobial, anticancer, antileishmanial, urease inhibition activities and interaction with SS-DNA of newly synthesized amide based carboxylic acid. Inorganica Chimica Acta 427:178–187
45. Mosmann T (1983) Rapid colorimetric assay for cellular growth and survival: application to proliferation and cytotoxicity assays. J Immunol Methods 65(1-2):55–63
46. Azam SS, Abbasi SW (2013) Molecular docking studies for the identification of novel melatoninergic inhibitors for acetylserotonin-O-methyltransferase using different docking routines. Theor Biol Med Model 24:63. doi:10.1186/1742-4682-10-63
47. Zhang H, Thomas R, Oupicky D, Peng F (2008) Synthesis and characterization of new copper thiosemicarbazone complexes with an ONNS quadridentate system: cell growth inhibition, S-phase cell cycle arrest and proapoptotic activities on cisplatin-resistant neuroblastoma cells. J Biol Inorg Chem 13:47–55
48. Naeimi H, Moradian M (2010) Synthesis and characterization of nitro-Schiff bases derived from 5-nitro-salicylaldehyde and various diamines and their complexes of Co(II). J Co Chem 63(1):156–162
49. Rajendiran V, Karthik R, Palaniandavar M, Evans HS, Periasamy VS, Akbarsha MA, Srinag BS, Krishnamurthy H (2007) Mixed-Ligand Copper(II)-phenolate complexes : Effect of coligand on enhanced DNA and protein binding, DNA cleavage, and anticancer activity. ACS Inorg Chem 46(20):8208–8221
50. Anupama B, Sunita M, Shiva Leela D, Ushaiah B, Gyana Kumari C (2014) synthesis, spectral characterization, DNA binding studies and antimicrobial activity of Co(II), Ni(II), Zn(II), Fe(III) and VO(IV) complexes with 4-Aminoantipyrine Schiff Base of Ortho-Vanillin. J Fluoresc 24:1067–1076
51. Raja DS, Bhuvanesh NSP, Natarajan K (2011) Effect of N(4)-Phenyl Substitution in 2-Oxo-1,2-dihydroquinoline-3-carbaldehyde semicarbazones on the structure, DNA/protein interaction, and antioxidative and cytotoxic activity of Cu(II) complexes.ACS. Inorg Chem 50:12852–12866
52. Barton JK, Raphaeln AL (1984) Photoactivated stereospecific cleavage of double helical DNA by cobalt (III) complexes. J Am Chem Soc 106:2466–2468
53. Jia L, Shi J, Sun Z, Li F, Wang Y, Wu W, Wang Q (2012) Synthesis, crystal structure, DNA-binding properties, cytotoxic and antioxidation activities of several ternary copper (II) complexes with a new reduced Schiff base. Inorganica Chimica Acta 391:121–129
54. Raman N, Mahalakshmi R, Arun T, Packianathan S (2014) Rajkumar R (2014) Metal based pharmacologically active complexes of Cu(II), Ni(II) and Zn(II): Synthesis, spectral, XRD, antimicrobial screening, DNA interaction and cleavage investigation. Journal of Photochem and Photobio B: Biology 138:211–222
55. Seeliger MA, Nagar B, Frank F, Cao X, Henderson MN, Kuriyan (2007) c-Src binds to the cancer drug imatinib with an inactive Abl/c-Kit conformation and a distributed thermodynamic penalty. J Structure 15:299–311
56. Li Z, Wan H, Shi Y, Ouyang P (2004) Personal experience with four kinds of Chemical structure drawing software: Review on chemdraw, chemwindow, draw, and chemsketch. J Chem Inf Comput Sci 44:1886–1890